Chapter V

Engineering Cobalt/Molybdenum Bimetallic MOF for Ultra-swift Detection of Uric Acid

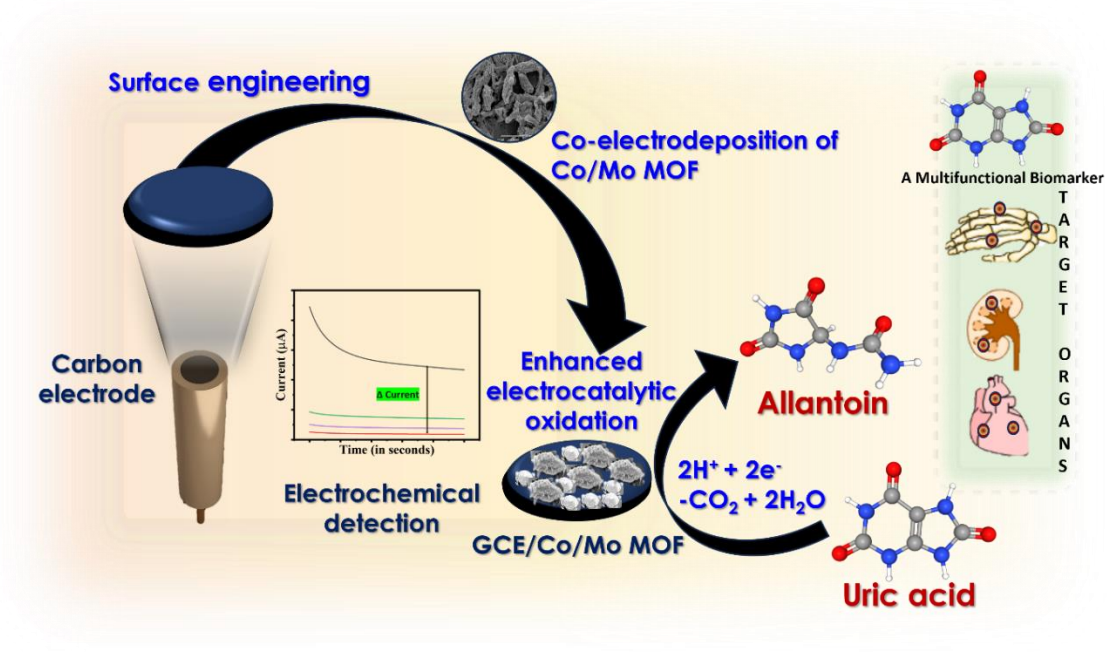

Shubhangi et al., 2024, IEEE Xplore, 10.1109/BioSensors61405.2024.10712685

1. Introduction

MOF, a class of self-assembled coordination complex-based porous materials, comprise of metal centre coordinated with organic linker moieties to form two or three-dimensional structures[1]. They have been designated as materials with high specific surface area, tunable mesoporosity, diverse catalytic metal centers linked to organic ligands with good adsorption affinities and superior redox behaviour[2]. These porous materials have found their utility in innumerable applications ranging from gas storage to catalysis and now to analytical applications like sensors and drug delivery systems[3]. However, the major challenges with working on these materials lies primarily with their wide band gap resulting into compromised electrochemical conductivity, heavily aggregated morphology and high resistance to diffusion[1]. Such phenomena have usually been observed in MOFs synthesized through the conventional solvothermal route which are now being replaced by newer synthesis protocols involving microwave, sonochemical and electrochemical methods[3]. MOFs have been projected as plausible solutions towards replacing enzyme-based sensors due to their catalytic metal centers imparting them with electrocatalytic potential[4]. Co-based MOFs have been recently reported as sensitive electrode matrix components for detection of analytes like UA[5].

Uric acid, a bio-compound also known as 2,6,8-trihydroxypurine, is often linked to various biophysiological pathways like purine (adenine and guanine) metabolism and decomposition. An abnormally high concentration or low concentration of UA is regarded as a causative factor for diseases like gout, hypertension, hyperuricemia, cardiovascular and chronic renal diseases, and oxidative stress. The clinical range of UA lies between 0.13-0.46 mM in blood serum and 1.49-4.46 mM in urine samples within healthy individuals. Therefore, a timely check on its physiological concentration holds enormous clinical significance in disease diagnosis. UA is routinely detected through enzyme-based

assays or alternatively through spectrometry and chromatography-based methods[6]. However, electrochemical non-enzymatic methods hold great promise for sensing UA due to faster response time, greater selectivity and cheaper operations. Although there always lies a scope for an alteration in sensor components which can improvise sensitivity and contribute towards realistic applications of the sensors.

In this work, we have attempted to fabricate a novel combination of Mo and Co-based bimetallic MOF within a sensor matrix for the selective and sensitive detection of UA through the electrochemical approach. The novelty lies in conjugation of two highly conductive metal centers conjugated with methyl imidazole linker moiety. The usual method of growing MOFs through the solvothermal approach followed by coating it onto a bare electrode surface is a complex operation which involves usage of binder components which may reduce the current response. We have tried to eliminate such problems by *in situ* growth of MOF onto the carbon electrode through a one-step electrodeposition procedure followed by testing it against our target analyte. The high conductivity and enormous surface area of the fabricated MOF matrix eliminates the need for further addition of successive conductive or catalytic components onto the surface, making it a simpler and effective solution for UA detection.

2. Materials and Methods

2.1. Chemicals and Instruments

Cobalt nitrate hexahydrate ($Co(NO_3)_2.6H_2O$), Dimethyl formamide (DMF), 2-methyl imidazole (2-MeIM), Potassium ferricyanide ($K_3Fe(CN)_6$), Potassium ferrocyanide ($K_4Fe(CN)_6.3H_2O$), Potassium chloride (KCl), Sodium chloride (NaCl), Sodium phosphate dibasic (Na_2HPO_4), Sodium phosphate monobasic (NaH_2PO4), were procured from SRL research laboratory, India. Molybdenum trioxide (MoO_3) was procured from

HiMedia Laboratories Pvt. Ltd. Distilled water (Milli-Q) (18 MΩ) was used throughout the experiment. The phosphate-buffered saline (PBS; 5 mM; pH 7.4) was prepared using a standard protocol.

2.2. Electrochemical Sensor Probe Characterization and Analytics

SEM and FTIR spectroscopy measurements were performed on JCM-6000 Plus BenchTop Sem Neoscope and Nicolet iS5, respectively availed at the Central Instrument Facility of IIT (BHU). All electrochemical operations required for facilitation of UA oxidation were performed on an electrochemical work station (Palm Sense BV, Houten, The Netherlands) connected to a three-electrode system constituting a bare glassy carbon electrode (GCE) as the working electrode, an Ag/AgCl as the reference electrode and, platinum wire as the counter electrode, respectively. CV was used for the electrochemical probe characterization and scan rate study by scanning between -0.2 V to +1.0 V vs. Ag/AgCl at a scan rate of 0.05 V/s in $[Fe(CN)_6]^{3-}/[Fe(CN)_6]^{4-}$ (ZoBell's) solution. ZoBell's solution was prepared through a pre-existing standard protocol[7–9].

2.3. Preparation and preliminary physical characterization of the Co/Mo MOF probe

GCE surface was cleaned and pretreated as per the standard protocol[10]. A solution containing 40 mM $(Co(NO_3)_2.6H_2O)$, 40 mM MoO_3, and 80 mM 2-MeIM were dissolved in 20 ml DMF and was stirred for 30 minutes to obtain the MOF precursor solution. The GCE electrode was then dipped into the precursor solution and scanned at a potential of -1.5 V for 500 seconds using chronoamperometry to deposit the Co/Mo MOF. The potential was optimised by performing experiments at varying potential points ranging from -0.4 V to -1.5 V. Similarly, the time for electrodeposition was optimised by performing the co-electrodeposition at fixed potential (-1.5 V) but at different time spans such as 100s, 200s, 300s, 500s and 700s. Post electrodeposition, the fabricated electrode

was rinsed with Milli-Q water and cured for 10 minutes at RT to obtain the final sensing probe.

2.4. Physical and electrochemical characterization of the nanoengineered Co/Mo MOF sensing probe

The probe was then subjected to physical characterisations like SEM and FTIR to confirm the formation of the bimetallic Co/Mo MOF. To confirm the presence of functional groups and binding of target metal center with the linker molecule, FTIR analysis was also done. The probe was then subjected to electrochemical measurements to deduce its electron transfer capabilities, as discussed in the upcoming sections.

2.5. Real Sample Analysis

The real-life application of the developed nanoengineered bimetallic sensing probe GCE/Co/Mo MOF was validated on synthetic serum samples. For the effective validation study on detection of UA, a conventional spike and recovery model was used. The synthetic serum was equilibrated with PBS by 10 times dilution and then spiked with varying concentrations of UA. This is a vital step to maintain the molar strength of the real matrix when compared with the standards to prove the sensor's performance. The recorded output current was plotted and compared with the calibration curve obtained from an initial concentration-dependent study on UA in standard buffer solutions.

3. Results and Discussion

3.1. Electrochemical nanoengineering and characterization of the GCE/Co/ sensing probe

An optimized synthesis of AuND was done through a simple yet robust electroimprinting technique to electrodeposit the Co/Mo bimetallic MOF. It was then characterized physically as well as electrochemically to validate its formation. Various physical

techniques were adopted at first stage to confirm the probe deposition of MOF layer such as SEM and FTIR analysis.

3.1.1. SEM and FTIR studies

The probe was subjected to physical characterisations like SEM and FTIR to confirm the formation of the bimetallic Co/Mo MOF, as seen in **Figure 5.1**. Below the magnification of 5 µm, spindle-shaped particles were seen evenly distributed on the entire topography of the electrode flanked with 2D spherical structures suggestive of desirable MOF-like patterns **(Figure 5.1-I)**. To confirm the presence of functional groups and binding of target metal center with the linker molecule, FTIR analysis was also done. Characteristic peaks corresponding to 2-MeIM moiety were seen between 690 to 1631 cm^{-1} suggesting its successful incorporation with the metal centers **(Figure 5.1-II).**

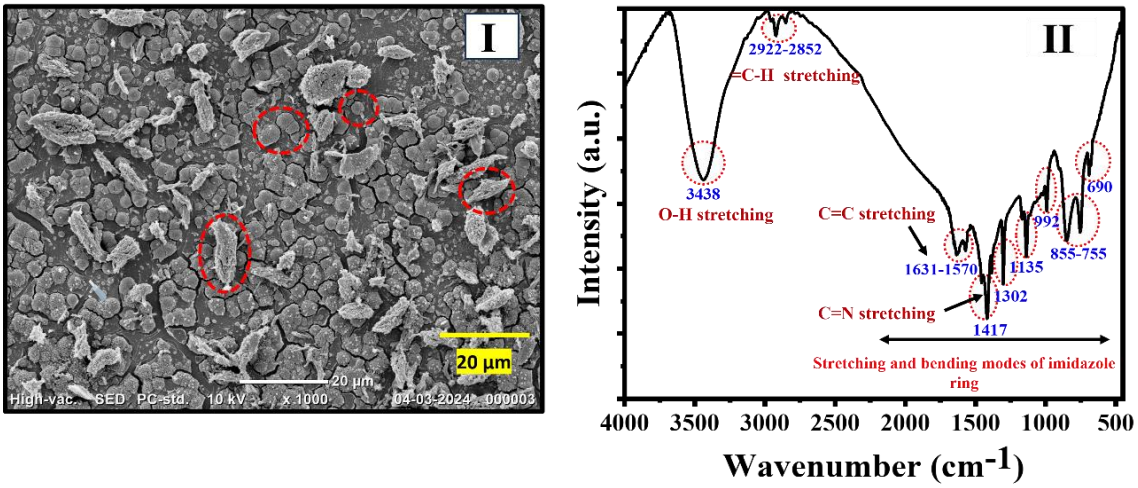

Figure 5.1. ***(I)*** *SEM micrograph of final fabricated electrode surface, i.e., Co/Mo MOF where red circles show spherical as well as spindle-shaped morphology of developed MOF particles.* ***(II)*** *FTIR spectrum of electrode/Co/Mo MOF.*

3.1.2. Electrochemical characterization of GCE/ Co/Mo MOF sensing probe

The developed final nanoengineered sensing surface GCE/Co/Mo MOF was electrochemically characterized through the CV measurements. Initially, the unmodified electrode surface was scanned in ZoBell's solution to obtain a characteristic peak of the (K_3[Fe (CN)$_6$]/K_4[Fe (CN)$_6$]) redox couple at +0.4V. The operations were performed

sequentially for both unmodified and modified GCE surfaces i.e., GCE, GCE/ Co/Mo MOF. At the first step, CV was performed in a potential range of -0.2 V to +1.0 V vs. Ag/AgCl with a scan rate of 50 mV/s in a 5 mM ZoBell's solution. **Figure 5.2-I** represents the CV signals for both surfaces where GCE is denoted through a black curve and GCE/Co/Mo MOF is represented by a red curve. Further the anodic and cathodic peaks currents have been represented through histogram in **Figure 5.2-I (inset)**. The final probe's surface charge transfer characteristics via quantification of the effective surface area was done using the Randles-Sevcik's equation

$$I_p = \left(2.69\times10^5\right) n^{3/2}\, ACD^{1/2}\, v^{1/2} \quad \text{.....Equation i}$$

where, Ip stands for the highest current output (in amperes), n denotes the no. of electrons involved in redox reaction (here n = 1), A stands for the electrodes' effective surface area (in cm^2), C is the electroactive species' concentration (in mole cm^{-3}), D demarcates the diffusion coefficient (in $cm^2\ s^{-1}$) with its value being constant, i.e., 7.6 × 10^{-6} cm^2s^{-1} for aqueous ferrocyanide, and v denotes the scan rate (in Vs^{-1}).

The effective surface area of GCE and GCE/Co/Mo MOF was found to be 6.15 x 10^{-5} cm^2 and 9.1 x 10^{-5} cm^2, respectively. There was an increase in the effective surface area of the probe by 1.48 times post modification with the bimetallic MOF component. Additionally, scan rate study for the final modified surface was performed to understand the mobility of ions and its stability by scanning within a potential window of -0.2 V and +1.0 V using CV with a varying scan rate (10-100 mV/s). The peak currents obtained at each scan rate were further plotted with current against the square root of scan rate in **Figure 5.2-II,** with the linear coefficients as 0.91 and 0.98 for the anodic and cathodic currents, respectively. The plotting results demonstrate a linear behaviour of the curve which clearly suggests that the electrode/electrolyte interface is a diffusion-controlled

process. The linearity obtained in this study also confirms the stable fabrication of final sensing surface (**Figure 5.2-II-inset)**.

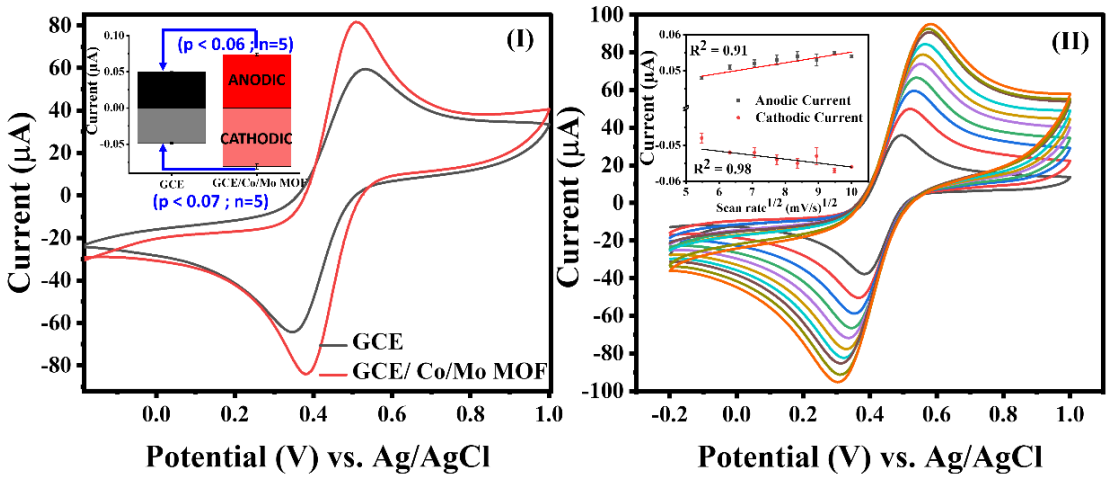

Figure 5.2. ***(I)*** *CV response of the modified surface at a scan rate of 50 mV/s in 5 mM ZoBell's solution* ***(I-inset)*** *Histogram representing the anodic and cathodic peak currents of the modified probe surface.* ***(II)*** *CV response of the final sensing probe GCE/Co/Mo MOF with varying scan rates (10-100 mV/s) in 5 mM ZoBell's solution* ***(II-inset)*** *Linear fit of the anodic and cathodic current vs. square root of scan rate.*

MOFs have always been known to hamper the conductivity of the sensor probe but in our case, interestingly, when the GCE surface was electrochemically deposited with Co/Mo bimetallic MOF through the novel route, a rise in conductivity was noted. Such electrodeposited MOF-dependent conductivity enhancement has been also observed earlier for different MOFs[11].

The great charge conducting capabilities of the nanoimprinted probe illuminates its enormous possibility in futures sensing applications.

3.2. Analytical performance of GCE/ Co/Mo MOF sensing probe

A set of comparative and control experiments were conducted to undermine the role of the MOF layer in the catalytic oxidation of UA. The obtained results can be seen through the generated data below. In the first set of control experiment, the data was generated for both unmodified and MOF-modified electrode surfaces against 20 mM UA concentration through LSV, by scanning between the potential window off +0.1 to +0.9 V vs. Ag/AgCl

(Figure 5.3-A). Since UA is an electroactive molecule, a distinct peak was obtained at around +0.65 V vs. Ag/AgCl for 20 mM UA, even in the case of a bare electrode surface, which gets shifted to a lower potential (+0.55 V) generating almost a double current response when oxidized by the MOF-modified probe.

Therefore, this engineered nanohybrid sensor probe brings out the inherent characteristics of MOF metal center (Co and Mo) for deployment in UA sensing application which may lead to its ultrasensitive detection without the need for more components in the sensing matrix.

The efficacy of the electrochemically developed sensing probe, GCE/ Co/Mo was analysed for its application by utilizing UA as a test molecule. The GCE/ Co/Mo nanoengineered sensing probe was subjected to a series of control experiments to establish that the increment in current magnitude with increase in potential was a resultant of direct and precise electron transfer with UA. In the first control experiment, a study was conducted at relatively higher concentrations of UA i.e., in 0.1 M to 0.5 M UA**.** In case of the blank reading, negligible intensity UA peak was seen, however, subsequently, current rose with increasing UA concentrations between 0.1 to 0.5 M **(Figure 5.3-C).** The curve shows a linear trend signifying concentration dependent signal, with a correlation coefficient of 0.98 **(Figure 5.3-D)**. The regression equation obtained from curve is as follows: $\Delta I\ (\mu A) = -8.277\ (\pm\ 3.453) + 2.757\ (\pm 0.167) \times$ Conc. [UA (M)].

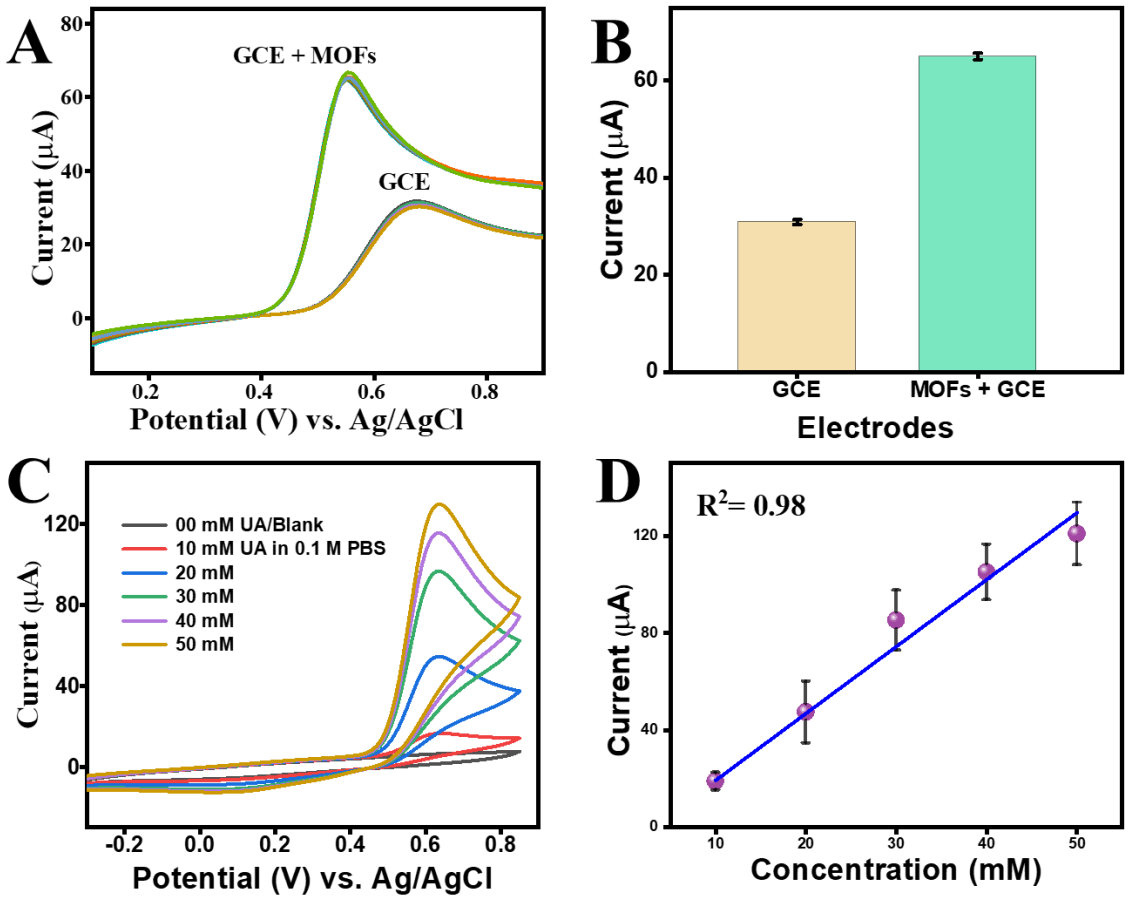

Figure 5.3. ***(A)*** *A comparative LSV curve corresponding to unmodified and modified (GCE/Co/Mo MOF) surface against PBS and 0.2 M UA dissolved in PBS.* ***(B)*** *Corresponding histogram generated from the layer-by-layer study, plotting the cathodic current response generated by the LSV curve measurements.* ***(C)*** *Concentration-dependent control analysis of GCE/Co/Mo probe in PBS* ***(black curve)****, and in 0.1 M* ***(red curve)****, 0.2 M* ***(blue curve)*** *and 0.3 M* ***(green curve),*** *0.4 M* ***(light purple curve)*** *and 0.5 M* ***(yellow curve)*** *UA to validate that peak is exclusively due to UA;* ***(D)*** *Corresponding calibration curve at varying concentrations ranging from 0.1 M to 0.5 M UA in PBS with correlation coefficients of 0.98.*

In the second control test, the charge transfer behaviour and stability of the analyte towards the GCE/Co/Mo bimetallic probe was analysed. It comprised of scan rate dependent study through an alteration in the scan rates between 10 and 100 mV/s in the presence of 10 mM UA **(Figure 5.4A)**. With an increment in scan rates, the cathodic peak currents also increased linearly. The engineered nanohybrid probe demonstrates diffusion-control charge transfer behaviour and excellent surface stability as the cathodic peak current was found to be proportional to the square root of scan rate possessing a correlation coefficient of 0.94 **(Figure 5.4B)**. Therefore, both the control studies inferred

that the designed GCE/Co/Mo engineered sensing probe is highly stable and can effectually sense UA.

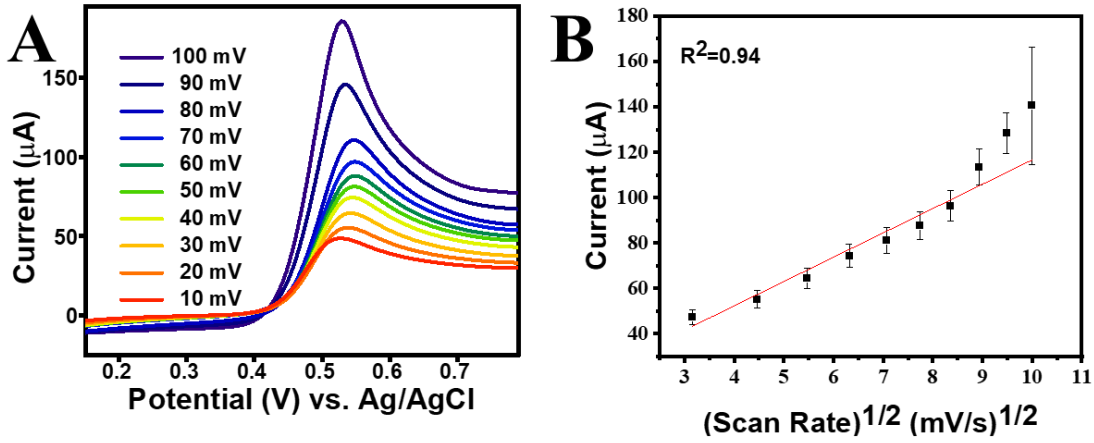

Figure 5.4. ***(A)*** *Scan rate dependent analysis of GCE/Co/Mo bimetallic engineered probe in 0.1M UA at a scan rate between 10 and 100 mV/s; As scan speeds increased, peak current rose with a small shift to the negative side;* ***(B)*** *corresponding current at different scan rates showed linearity with a correlation coefficient of 0.94.*

The sensing capabilities of the probe were further investigated using DPV to find the minimal concentration since DPV is considered as a highly sensitive technique. The GCE/Co/Mo probe was evaluated for varying concentrations of UA and the signal output was found to be increasing with an increase in UA levels **(Figure 5.5A)**. On the basis of the amperometry data, the calibration curve showcased a linearity within the concentration range of 1 x 10^{-2} to 1 x 10^{-9} M **(Figure 5.5B)**. The LOD of UA was calculated as 0.34 (±0.05) x 10^{-10} M using **equation ii**

$$LOD = \frac{3\mathrm{SD}_b}{Slope} = \frac{3\mathrm{SD}_b}{\frac{dy}{dx}} = \frac{3\mathrm{SD}_b}{\frac{dy}{dlnx} \times \frac{dlnx}{dx}} = \frac{3\mathrm{SD}_b}{\frac{dy}{2.303(dlogx)} \times \frac{1}{x}}$$

$$= \frac{3 \times 2.303 \times \mathrm{SD}_b \times x}{\frac{dy}{dlogx}} = \frac{3 \times 2.303 \times \mathrm{SD}_b \times x}{Slope\ of\ semilog\ plot}$$

…….Equation ii

where σ_b represents the blank sample's standard deviation, and m is the calibration plot's slope

The linear increment in DPV current responses with rise in UA concentrations in between 1 x 10^{-7} to 1 x 10^{-9} M can be summed up through the regression equations shown below:

Regression equation 1: For lower concentration range

$$I\ (\mu A) = 6.447\ (\pm 1.047) + 0.660\ (\pm 0.117) \times [\log \text{Conc. of UA (M)}].$$

Regression equation 2: For higher concentration range

$$I\ (\mu A) = 46.116\ (\pm 2.561) + 8.645\ (\pm 0.791) \times [\log \text{Conc. of UA (M)}].$$

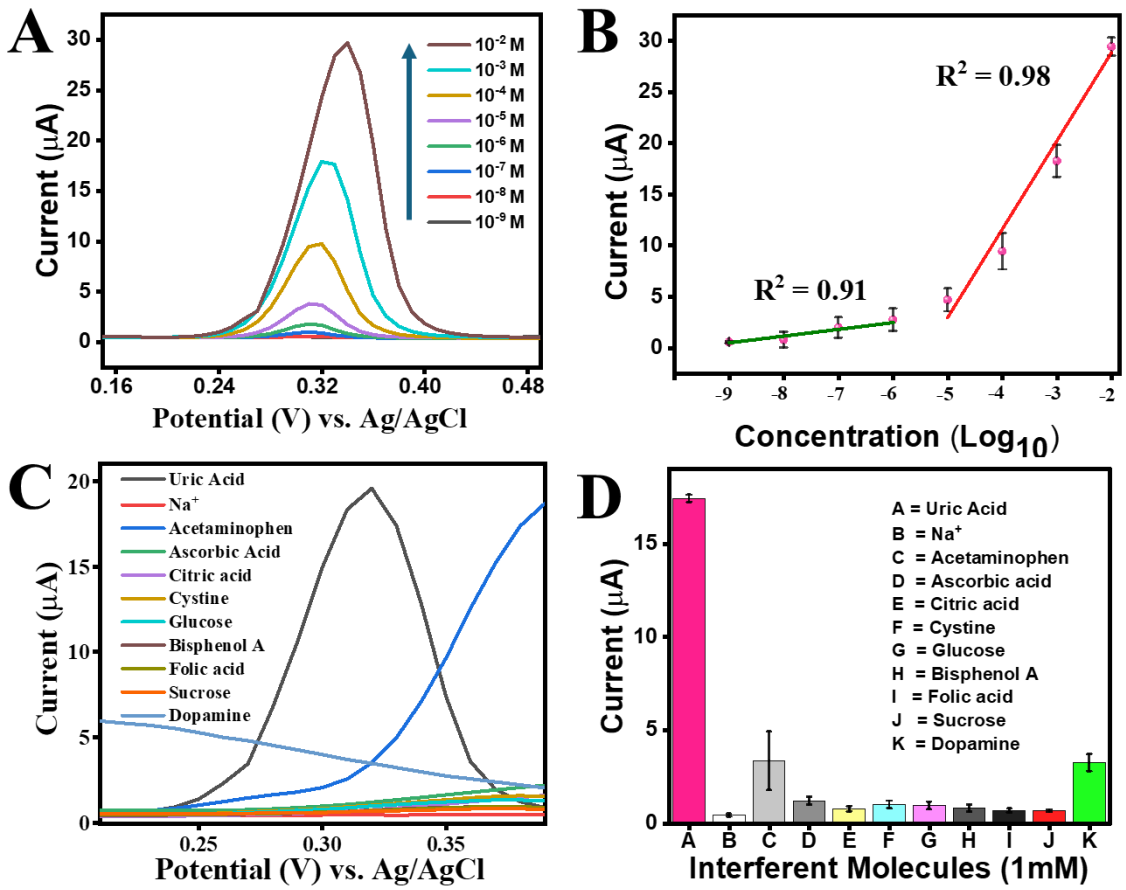

Figure 5.5. ***(A)*** *The DPV response of GCE/Co/Mo bimetallic MOF-based sensor probe in the range of 1 x 10^{-2} to 1 x 10^{-9} M UA in PBS to find the minimal concentration of UA;* ***(B)*** *Corresponding calibration curve of varying concentrations of UA in PBS with a correlation coefficient of 0.94 for 10^{-7} to 10^{-9} M UA as 0.91 and 10^{-2} to 10^{-5} M UA is 0.98, respectively;* ***(C)*** *Interference analysis study* ***(D)*** *Interference study histogram.*

3.3. Selectivity assay

The commercial applications of the developed GCE/Co/Mo nano-engineered probe requires proving its selectivity towards the specific target analyte present amongst many

co-existing interferant molecules within a complex matrix. Therefore, we chose various co-existing molecules such as sodium ions (Na^+), acetaminophen, ascorbic acid, citric acid, cysteine, glucose, bisphenol A, folic acid, sucrose, dopamine along with our target analyte UA, to examine nanohybrid sensing probe's selectivity. **Figure 5.5-C** highlights the signal response of the co-existing molecules which displayed minimal signals at around +0.32 V vs. Ag/AgCl. **equation iii** was used to determine the coefficient of selectivity (K_{sel}) of the co-existing molecules, with their respective values stated in **Table 5.1**. The values were found to be significantly low ($K_{sel.}$ <<1), with p-value <0.02 emphasizing good selectivity of the developed GCE/Co/Mo bimetallic MOF probe for UA analysis.

$$K_{sel.} = (Signal)_{Interfering\ molecules} / (Signal)_{UA} \quad \ldots Equation\ iii$$

where $K_{sel.}$ denotes the coefficient of selectivity, $(Signal)_{interfering\ molecules}$ are the current corresponding to interferants, and $(Signal)_{H2O2}$ is the response generated by the nanoprobe after being treated with UA.

Table 5.1. *Coefficient of selectivity (K_{sel}) of the co-existing interferant molecules*

Co-existing molecules	Current Signal (μA)	$K_{sel.}$
Na^+	*0.409*	*0.023*
Acetaminophen	*3.324*	*0.190*
Ascorbic Acid	*1.183*	*0.067*
Cysteine	*0.978*	*0.056*
Citric Acid	*0.743*	*0.042*
Glucose	*0.925*	*0.053*
Bisphenol A	*0.784*	*0.044*
Folic Acid	*0.409*	*0.023*
Dopamine	*3.228*	*0.185*
Uric Acid	*17.423*	*1*

No significant response was recorded for the co-existing interferants in our experiments due to the electrochemical passivity of developed GCE/Co/Mo probe towards these

molecules. Another reason could be the analytical potential range, which forbidden other electroactive species from experiencing the redox reaction. The developed sensor has been compared with other MOF-based state-of-the-art sensors developed for the detection of UA so far in **Table 5.2.** It is quite evident that the currently developed BMOF-based sensor not only covers a broader LDR but also is more sensitive in terms of its LOD when compared to the latest reports on electrochemical UA detection.

4. Conclusion

We have developed a bimetallic MOF based nanocomposite (GCE/Co/Mo MOF) through the electrochemical route for the electro-catalytic oxidation and thereby sensing of UA. Co/Mo-MOF was electrochemically deposited on the GCE surface using a one-step approach where a stable catalytic layer suffices the need for UA detection. Physical characterization tools like SEM and FTIR were adopted for confirming the formation of the target MOF. These methods were also supplemented by electrochemical techniques such as CV, DPV and CA to characterize as well as understand the analytical potential of developed probe. The synergistic effect of Co/Mo MOF results in an electroconductive surface facilitating enhanced oxidation of the target analyte. The developed nanocomposite was used to detect UA concentration electrochemically in the known clinical ranges. The future prospects could also be integration of the proposed matrix in wearable and patch-based sensors which would however require advance analyses involving the toxicity aspects of these materials. This is a preliminary study which may further help in exploring applicability of such MOFs in integration with other catalytic surfaces for the detection of a range of clinically significant analytes.

Table 5.2. *Comparative report on the developed sensor's analytical parameters with recently developed MOF-based UA sensors.*

S.No.	Fabricated probe surface	Technique used	LDR	LOD	Real Sample used	Ref.
1.	ZIF-8 and ZIF-67 based BMOF system	DPV	2-110 μM	0.83 μM	Human serum samples	[12]
2	MOF-71	CV, DPV	50-1000 μM	15.61 μM	N.R.	[13]
3.	Ce-MOF	CV, DPV	1.50-2.50 μM	CV:0.26 × 10^{-3} M; DPV: 0.9 × 10^{-6}M	Serum	[14]
4.	ZIF-67	CV, DPV	20-1000 μM	3.04 μM	N.R.	[4]
5.	Au@Ni-MOF	DPV, EIS	10-1000 μM	0.19 μM	Urine	[15]
6.	Au@Cu-MOF	DPV	0.9 μM- 18.9 μM	10.36 μM	Urine and serum	[16]
7.	Ni-MOF-74	DPV	0- 6.0 μM	70 nM	N.R.	[17]
8.	ZIF-8 nano ZIFs	DPV	0.01-2800 μM	5.6 nM	Normal or hyperuricemia serum	[18]
9.	Co-MOF	DPV	0.4- 400 μM	3.4 ppb	Serum	[6]
10.	Cu-BTC MOF	DPV	0.05-500.0 μM	0.2 μM	Urine	[19]
11.	***Co-Mo BMOF***	***DPV***	***10^{-7}- 10^{-9} M UA and 10^{-2}-10^{-5} M UA***	***0.34 (±0.05) x 10^{-10} M***	***NA***	***This work***

REFERENCES

(1) Ahmad, M. W.; Dey, B.; Sarkhel, G.; Yang, D.-J.; Choudhury, A. Sea-Urchin-like Cobalt-MOF on Electrospun Carbon Nanofiber Mat as a Self-Supporting Electrode for Sensing of Xanthine and Uric Acid. *J. Electroanal. Chem.* **2022**, *920*. https://doi.org/10.1016/j.jelechem.2022.116646.

(2) Shubhangi, N.; Kumari, R.; Rai, S. K.; Chandra, P. Electrochemical Assembly of Nickel Metal Organic Framework-Decorated Nanoimprinted Gold Dendrites as Peroxidase Mimic for High-Performance Hydrogen Peroxide Sensing. *ACS Appl. Nano Mater.* **2024**, *7* (1), 1388–1401. https://doi.org/10.1021/acsanm.3c05396.

(3) Shubhangi; Nandi, I.; Rai, S. K.; Chandra, P. MOF-Based Nanocomposites as Transduction Matrices for Optical and Electrochemical Sensing. *Talanta* **2024**, *266* (P2), 125124. https://doi.org/10.1016/j.talanta.2023.125124.

(4) Abrori, S. A.; Septiani, N. L. W.; Nugraha; Nuruddin, A.; Anshori, I.; Yuliarto, B. Comparison of a 2D/3D Imidazole-Based MOF and Its Application as a Non-Enzymatic Electrochemical Sensor for the Detection of Uric Acid. *New J. Chem.* **2022**, *46* (44), 21342–21349. https://doi.org/10.1039/D2NJ02664C.

(5) Xu, F.; Wang, L.; Wu, M.; Ma, G. Vertical Growth of Leaf-like Co-Metal Organic Framework on Carbon Fiber Cloth as Integrated Electrode for Sensitive Detection of Dopamine and Uric Acid. *Sensors Actuators B Chem.* **2023**, *386*, 133734. https://doi.org/https://doi.org/10.1016/j.snb.2023.133734.

(6) Wang, F.; Zhao, D.; Li, W.; Zhang, H.; Li, B.; Hu, T.; Fan, L. Rod-Shaped Units Based Cobalt(II) Organic Framework as an Efficient Electrochemical Sensor for Uric Acid Detection in Serum. *Microchem. J.* **2023**, *185*. https://doi.org/10.1016/j.microc.2022.108154.

(7) Purohit, B.; Mahato, K.; Kumar, A.; Chandra, P. Sputtering Enhanced Peroxidase like Activity of a Dendritic Nanochip for Amperometric Determination of Hydrogen Peroxide in Blood Samples. *Microchim. Acta* **2019**, *186* (9), 658. https://doi.org/10.1007/s00604-019-3773-2.

(8) Chung, S.; Chandra, P.; Koo, J. P.; Shim, Y.-B. Development of a Bifunctional Nanobiosensor for Screening and Detection of Chemokine Ligand in Colorectal Cancer Cell Line. *Biosens. Bioelectron.* **2018**, *100*, 396–403. https://doi.org/https://doi.org/10.1016/j.bios.2017.09.031.

(9) Purohit, B.; Kumar, A.; Mahato, K.; Chandra, P. Novel Sensing Assembly Comprising Engineered Gold Dendrites and MWCNT-AuNPs Nanohybrid for Acetaminophen Detection in Human Urine. *Electroanalysis* **2020**, *32* (3), 561–570. https://doi.org/10.1002/elan.201900551.

(10) Kumar, A.; Purohit, B.; Mahato, K.; Mandal, R.; Srivastava, A.; Chandra, P. Gold-Iron Bimetallic Nanoparticles Impregnated Reduced Graphene Oxide Based Nanosensor for Label-Free Detection of Biomarker Related to Non-Alcoholic Fatty Liver Disease. *Electroanalysis* **2019**, *31* (12), 2417–2428. https://doi.org/10.1002/elan.201900337.

(11) Han, S.; Sun, R.; Zhao, L.; Yan, C.; Chu, H. Molecularly Imprinted Electrochemical Sensor Based on Synergistic Interaction of Honeycomb-like Ni-MOF Decorated with AgNPs and N-GQDs for Ultra-Sensitive Detection of Olaquindox in Animal-Origin Food. *Food Chem.* **2023**, *418* (March), 136001. https://doi.org/10.1016/j.foodchem.2023.136001.

(12) Liu, L.; Liu, L.; Wang, Y.; Ye, B.-C. A Novel Electrochemical Sensor Based on Bimetallic Metal–Organic Framework-Derived Porous Carbon for Detection of Uric Acid. *Talanta* **2019**, *199*, 478–484. https://doi.org/https://doi.org/10.1016/j.talanta.2019.03.008.

(13) Abrori, S. A.; Septiani, N. L. W.; Hakim, F. N.; Maulana, A.; Suyatman; Nugraha; Anshori, I.; Yuliarto, B. Non-Enzymatic Electrochemical Detection for Uric Acid Based on a Glassy Carbon Electrode Modified With MOF-71. *IEEE Sens. J.* **2021**, *21* (1), 170–177. https://doi.org/10.1109/JSEN.2020.3014298.

(14) Saeed, U.; Fatima, B.; Hussain, D.; Imran, M.; Jamil, M.; Naeem Ashiq, M.; Najam-ul-Haq, M. Scalable Synthesis of Ce-MOF Derived CeO/C Hierarchical: Efficient Electrochemical Sensing of Uric Acid as Potential Biomarker in Acute Myeloid Leukaemia Patients. *Microchem. J.* **2022**, *181*, 107808. https://doi.org/https://doi.org/10.1016/j.microc.2022.107808.

(15) Zhou, F.; Gai, L.; Liu, H.; Qin, D.; Abudouwufu, T.; Liu, Y. Enhanced Electrochemical Detection of Dopamine and Uric Acid Using Au@Ni-MOF and Employing 2D Structure DFT Simulation. *Sci. Rep.* **2025**, *15* (1), 8686. https://doi.org/10.1038/s41598-025-89797-1.

(16) Zhou, F.; Lim, H. N.; Ibrahim, I.; Endot, N. A.; Malek, E. A.; Gowthaman, N. S. K. Simultaneous Electrochemical Detection of Dopamine and Uric Acid via Au@Cu-Metal Organic Framework. *Chempluschem* **2024**, *89* (5), e202300686. https://doi.org/https://doi.org/10.1002/cplu.202300686.

(17) Li, G.; Liu, S.; Liu, D.; Zhang, N. MOF-Derived Porous Nanostructured Ni2P/C Material with Highly Sensitive Electrochemical Sensor for Uric Acid. *Inorg. Chem. Commun.* **2021**, *130*, 108713. https://doi.org/https://doi.org/10.1016/j.inoche.2021.108713.

(18) Xie, X.; Mo, G.; Hu, B. Electrochemical Assembling of Nano-MOFs at Carbon Fiber for the High-Performance Uric Acid Sensing. *Sensors Actuators B Chem.* **2023**, *393*, 134263. https://doi.org/https://doi.org/10.1016/j.snb.2023.134263.

(19) Azizpour Moallem, Q.; Beitollahi, H. Electrochemical Sensor for Simultaneous Detection of Dopamine and Uric Acid Based on a Carbon Paste Electrode Modified with Nanostructured Cu-Based Metal-Organic Frameworks. *Microchem. J.* **2022**, *177*, 107261. https://doi.org/https://doi.org/10.1016/j.microc.2022.107261.